OFFPRINT

g-factor measurements at RISING: The cases of ^{127}Sn and ^{128}Sn

L. Atanasova, D. L. Balabanski, S. K. Chamoli, M. Hass, G. S. Simpson, D. Bazzacco, F. Becker, P. Bednarczyk, G. Benzoni, N. Blasi, A. Blazhev, A. Bracco, C. Brandau, L. Caceres, F. Camera, F. C. L. Crespi, P. Detistov, P. Doornenbal, C. Fahlander, E. Farnea, G. Georgiev, J. Gerl, K. A. Gladnishki, M. Górska, J. Grebosz, R. Hoischen, G. Ilie, M. Ionescu-Bujor, A. Iordachescu, A. Jungclaus, G. Lo Bianco, M. Kmiecik, I. Kojouharov, N. Kurz, S. Lakshmi, R. Lozeva, A. Maj, D. Montanari, G. Neyens, M. Pfützner, S. Pietri, Zs. Podolyák, W. Prokopowicz, D. Rudolph, G. Rusev, T. R. Saito, A. Saltarelli, H. Schaffner, R. Schwengner, S. Tashenov, J. J. Valiente-Dobón, N. Vermeulen, J. Walker, E. Werner-Malento, O. Wieland, H. J. Wollersheim, H. Grawe and M. Hjorth-Jensen

Please visit the new website
www.epljournal.org

TARGET YOUR RESEARCH WITH EPL

Sign up to receive the free EPL table of contents alert.

www.epljournal.org/alerts

g-factor measurements at RISING: The cases of ^{127}Sn and ^{128}Sn

L. Atanasova[1(a)], D. L. Balabanski[1,2], S. K. Chamoli[3], M. Hass[3], G. S. Simpson[4], D. Bazzacco[5],
F. Becker[6], P. Bednarczyk[6,7], G. Benzoni[8], N. Blasi[8], A. Blazhev[9], A. Bracco[8], C. Brandau[6,10],
L. Caceres[6], F. Camera[8], F. C. L. Crespi[8], P. Detistov[1], P. Doornenbal[6], C. Fahlander[11],
E. Farnea[5], G. Georgiev[12], J. Gerl[6], K. A. Gladnishki[2,13], M. Górska[6], J. Grebosz[6,7], R. Hoischen[11],
G. Ilie[9,14], M. Ionescu-Bujor[14], A. Iordachescu[14], A. Jungclaus[15], G. Lo Bianco[2], M. Kmiecik[7],
I. Kojouharov[6], N. Kurz[6], S. Lakshmi[3], R. Lozeva[13,16], A. Maj[7], D. Montanari[8], G. Neyens[16],
M. Pfützner[17], S. Pietri[10], Zs. Podolyák[10], W. Prokopowicz[6,7], D. Rudolph[11], G. Rusev[18],
T. R. Saito[6], A. Saltarelli[2], H. Schaffner[6], R. Schwengner[18], S. Tashenov[6], J. J. Valiente-Dobón[19],
N. Vermeulen[16], J. Walker[6,10], E. Werner-Malento[6,17], O. Wieland[8], H. J. Wollersheim[6], H. Grawe[6]
and M. Hjorth-Jensen[20]

[1] *Institute for Nuclear Research and Nuclear Energy, Bulgarian Academy of Sciences - BG-1784 Sofia, Bulgaria, EU*
[2] *Physics Division, School of Science and Technology, Università di Camerino and INFN, Sezione di Perugia*
I-62032 Camerino (Macerata), Italy, EU
[3] *Weizmann Institute of Science - Rehovot 76100, Israel*
[4] *LPSC, Université Joseph Fourier Grenoble 1, CNRS/IN2P3, Institut National Polytechnique de Grenoble*
F-38026 Grenoble Cedex, France, EU
[5] *Dipartimento di Fisica, Università di Padova and INFN, Sezione di Padova - I-35131 Padova, Italy, EU*
[6] *GSI Helmholtzzentrum für Schwerionenforschung GmbH - Planckstr. 1, D-64291 Darmstadt, Germany, EU*
[7] *The Henryk Niewodniczański Institute of Nuclear Physics, PAN - PL-31342 Kraków, Poland, EU*
[8] *Dipartimento di Fisica, Università degli Studi di Milano and INFN, Sezione di Milano - I-20133 Milano, Italy, EU*
[9] *IKP, Universität zu Köln - D-50937, Köln, Germany, EU*
[10] *Department of Physics, University of Surrey - Guildford, GU2 7XH, UK, EU*
[11] *Department of Physics, Lund University - S-22100 Lund, Sweden, EU*
[12] *CSNSM, Université Paris-Sud 11, CNRS/IN2P3 - F-91405 Orsay-Campus, France, EU*
[13] *Faculty of Physics, St. Kliment Ohridski University of Sofia - BG-1164 Sofia, Bulgaria, EU*
[14] *Horia Hulubei National Institute of Physics and Nuclear Engineering - R-077125, Bucharest, Romania, EU*
[15] *Instituto de Estructura de la Materia, CSIC - E-28006 Madrid, Spain, EU*
[16] *Instituut voor Kern- en Stralingsfysica, K.U. Leuven - Celestijnenlaan 200D, B-3001 Leuven, Belgium, EU*
[17] *IEP, Warsaw University - PL-00681 Warsaw, Poland, EU*
[18] *Institut für Strahlenphysik, FZ Dresden-Rossendorf - D-01314, Dresden, Germany, EU*
[19] *INFN - Laboratori Nazionali di Legnaro - I-35020 Legnaro (Padova), Italy, EU*
[20] *Department of Physics and Centre of Mathematics for Applications, University of Oslo - N-0316 Oslo, Norway*

Abstract – We report on g-factor measurements of the $19/2^+$ $T_{1/2} = 4.5(3)\,\mu$s isomer in ^{127}Sn
and the 10^+ $T_{1/2} = 2.69(23)\,\mu$s isomer in ^{128}Sn. These isomers were produced and spin-aligned
in relativistic heavy-ion fragmentation at GSI and were selected and separated by the GSI
fragment separator (FRS). The γ-rays of the isomeric decay were detected by the RISING γ-ray
spectrometer. The method of time-differential perturbed angular distributions was utilized. The
measured g-factors, $g(19/2^+;\ ^{127}$Sn$) = -0.17(2)$ and $g(10^+;\ ^{128}$Sn$) = -0.20(4)$, are compared
with shell model calculations. The measured g-factors confirm the predominantly $\nu h_{11/2}^{-2}$ and
$\nu(s_{1/2}^{-1} h_{11/2}^{-2})$ character of the 10^+ and $19/2^-$ isomers in ^{128}Sn and ^{127}Sn, respectively. The results
demonstrate the feasibility of the method for similar measurements in exotic neutron-rich nuclei.
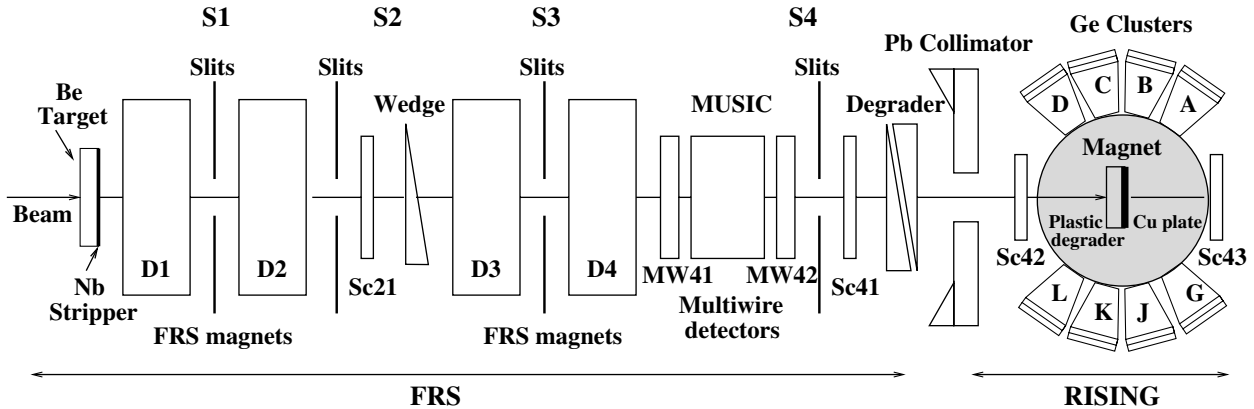
(a)E-mail: liliya@inrne.bas.bg

Fig. 1: Schematic view of the experimental set-up (see text): the fragment separator (FRS) with the beam-tracking detectors, the RISING γ-ray detectors (A–D) and (G–L), the electromagnet and the implantation detectors.

Introduction. – Nuclei in the vicinity of closed proton and neutron shells exhibit simple single-particle excitation spectra, with rather pure wave functions. This is due to the fact that there are only few levels close to the Fermi surface and configuration mixing effects, resulting from particle-hole excitations across the shell gaps, are suppressed to a great extent [1]. However, the nuclear shell model traditionally was established and critically tested for nuclei close to the region of stability. It is, therefore, important for a further understanding of the nuclear shell structure to study nuclei in the vicinity of closed proton and neutron shells away from the valley of β-stability, such as $^{132}_{50}\mathrm{Sn}_{82}$ or $^{78}_{28}\mathrm{Ni}_{50}$.

Nuclear g-factors play a special role in such a quest since they provide information about the configuration of the states of interest. In particular, in the vicinity of doubly magic nuclei, they shed light on the purity of the nuclear wave function, reflecting the stability of nuclear shells.

A possibility to investigate neutron-rich nuclei is provided by projectile fragmentation. So far, such reactions were utilized for studies of isomeric moments in nuclei with $A \leqslant 70$ [2–7]. The spin-orientation of the isomeric ensemble is produced in the reaction itself. To preserve as much alignment as possible only fully stripped nuclei are selected during the flight through a separator. In such a way perturbation effects, due to the hyperfine interaction with the randomly oriented electron spin, are avoided. Within the RISING (Rare ISotope INvestigations @ GSI) γ array project [8] g-factor measurements of heavier nuclei were performed [9], taking advantage of the relativistic beams at GSI.

The cases under study are microsecond isomers in the neutron-rich Sn isotopes, which have a magic number of protons $Z = 50$. The structure of Sn isotopes in the vicinity of $^{132}\mathrm{Sn}$ with neutron numbers $N < 82$ is governed by neutron hole configurations in the negative-parity $1h_{11/2}$ and the positive-parity $2d_{3/2}$ and $3s_{1/2}$ orbitals. Microsecond isomers are known in the spectra of the even-A and odd-A Sn isotopes with $N < 82$, correspondingly [10]. The 10^+ microsecond isomers with a leading configuration of

$\nu 1h_{11/2}^{-2}$ and seniority $\nu = 2$ are observed experimentally in the Sn isotopes in the mass range $A = 116$–130 [10]. Three quasiparticle $19/2^+$ isomers were observed for the odd-A Sn nuclei with masses between $A = 119$ and $A = 129$ [10]. The $\nu(3s_{1/2}^{-1}1h_{11/2}^{-2})_{19/2^+}$ configuration was assigned to them [11].

This paper reports a measurement of the g-factors of the $19/2^+$ isomer with $T_{1/2} = 4.5(3)\,\mu\mathrm{s}$ in $^{127}\mathrm{Sn}$ [11] and the 10^+ isomer with $T_{1/2} = 2.69(23)\,\mu\mathrm{s}$ in $^{128}\mathrm{Sn}$ [12] and addresses the ensuing shell model interpretation. Preliminary results for $^{127}\mathrm{Sn}$ were published in conference proceedings [13,14].

Experimental technique and results. – Neutron-rich nuclei around $A \approx 130$ were produced and spin-oriented in relativistic projectile fragmentation of a $^{136}\mathrm{Xe}$ beam at $E/A = 600\,\mathrm{MeV}/A$ on a $1024\,\mathrm{mg/cm^2}$ Be production target. The primary beam was provided by the GSI heavy-ion synchrotron (SIS) with an average intensity of about $10^8\,\mathrm{ions/s}$ ($2 \cdot 10^9$ ions per $10\,\mathrm{s}$ spill with a $18\,\mathrm{s}$ repetition period). The fully stripped ions were separated and identified with the two-stage high-resolution magnetic zero-degree FRagment Separator (FRS) [15], which was operated in the standard achromatic mode.

A schematic view of the experimental set-up is shown in fig. 1. The fragment selection was optimized for $^{127}\mathrm{Sn}$. The nuclei of interest were tracked and identified on an event-by-event basis. The mass-to-charge ratio, A/q, was determined by measuring the time of flight with scintillator detectors Sc21 and Sc41 (see fig. 1) and the magnetic rigidity of the beam, $B\rho$. Since the Sn isotopes of interest have A/q values rather close to the primary beam, it was necessary to introduce slits at the S2 position of the FRS in order to cut the primary beam and to optimize the load of the position-sensitive scintillator Sc21, limiting its rate to below $10^6\,\mathrm{ions/s}$. The ionic charge, Z, was determined by the energy loss in the MUlti-Sampling Ionization Chamber (MUSIC) at the final focus, S4. A typical identification plot of the ions which reach the final focus of the FRS, in the present experiment, is shown in fig. 2(a).
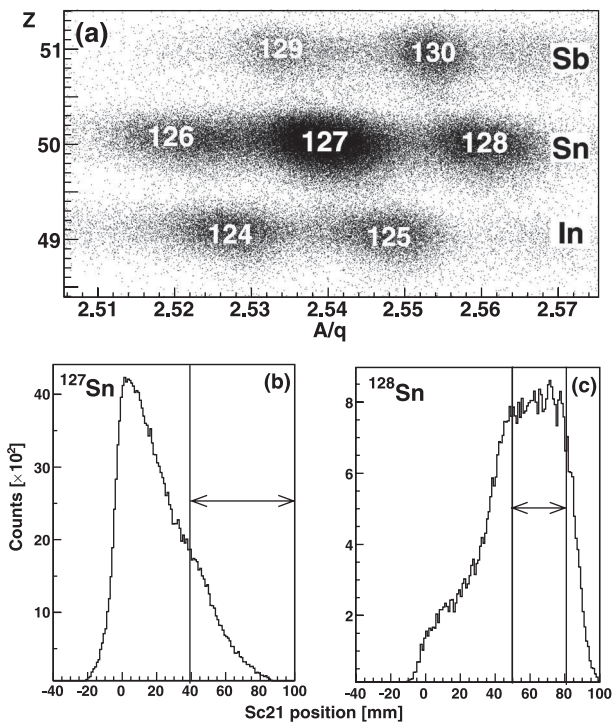
Fig. 2: (a) Ion identification plot. The spots corresponding to different isotopes are labelled with the isotope notation; (b) longitudinal momentum distribution for ^{127}Sn; (c) longitudinal momentum distribution for ^{128}Sn. The momentum distribution is measured with Sc21. The vertical lines in (b) and (c) indicate the momentum selection, which was used in the data analysis.

Fig. 3: (a) Partial level scheme of ^{127}Sn showing the decay of $19/2^+$ isomer. (b) Energy spectrum for ^{127}Sn and ^{128}Sn gated on the identification plot. The labelled transitions belong to the decay of the $19/2^+$ isomer in ^{127}Sn and 10^+ isomer in ^{128}Sn. Unlabled transitions are due to different interactions of the beam with the set-up materials and natural radioactivity. (c) Partial level scheme of ^{128}Sn showing the decay of 10^+ isomer.

beam-tracking detectors and the isomeric γ-rays were used as trigger of the data acquisition system in the experiment. The data analysis was done with the SPY/CRACOW [17] and ROOT [18] software. Transitions belonging to the isomeric decay of ^{127,128}Sn can be clearly identified in the γ-ray spectrum in fig. 3. The rapid drop of intensity below 150 keV is due to absorbers that were mounted in front of the Ge detectors in order to suppress the prompt bremsstrahlung flash. Partial level schemes, revealing the isomeric decay of ^{127,128}Sn, are presented in fig. 3(a), (c). Note that the spin-parity assignments in ^{127}Sn are based on the similarity with the level schemes for the lighter Sn isotopes and theoretical calculations [11].

The method of the time-differential perturbed angular distribution (TDPAD) [4,19] was used for the determination of the g-factors of the isomers in ^{127,128}Sn. The spin-oriented isomeric ensemble was implanted in a Cu cubic lattice host. It was placed between the poles of an electromagnet that generated a constant magnetic field $\vec{B}$ in a vertical direction, $B = 0.1200(3)$ T. As a result, the isomeric spin ensemble precesses around the magnetic field with a Larmor frequency $\omega_L = -gB\mu_N/\hbar$, which depends on the value of the magnetic-field strength, B, and the isomeric g-factor.

The intensity of the isomeric transitions was recorded as a function of time. The $t = 0$ signal was generated by an ion impinging on the plastic scintillator Sc41. The frequency of the Larmor precession was extracted from the measured time spectra by sorting experimental $R(t)$ functions for each γ transition, using detectors positioned at symmetric angles, θ and $\theta + \pi$, with respect to the beam line. The $R(t)$-function is defined as

$$R(t, \theta, \omega_L) = \frac{I(t, \theta, \omega_L) - \epsilon I(t, \theta + \pi/2, \omega_L)}{I(t, \theta, \omega_L) + \epsilon I(t, \theta + \pi/2, \omega_L)}$$

$$= \frac{3A_2B_2}{4 + A_2B_2} \sin(2\omega_L t), \qquad (1)$$

The isomeric ensemble produced in the projectile fragmentation reaction is spin-oriented, provided that only a specific part of the longitudinal momentum distribution is selected, with prolate alignment at the center and oblate alignment at the wing [2]. The momentum distribution of the fragments was measured by the position-sensitive scintillator detector Sc21 at the second focal plane of FRS (see fig. 1). The momentum distributions for ^{127,128}Sn, which were measured with the FRS setting of the experiment, are presented in fig. 2(b), (c). An asymmetric S2 slit was used in order to suppress the primary beam. It cuts also parts of the momentum distribution for ^{127}Sn (the left wing and part of the center) and ^{128}Sn (the leftmost wing and the right wing).

The selected ions were implanted in a high-purity (99.998%) 2 mm annealed copper plate, fixed to a thick plastic degrader to guarantee that the ions of interest are stopped in the Cu [9]. The Sc42 and Sc43 detectors were used for control of the implantation. The isomeric γ-rays were measured with eight cluster Ge detectors, mounted in the horizontal plane. They were placed at angles of $\pm 45°$, $\pm 75°$, $\pm 105°$ and $\pm 135°$ with respect to the beam direction. Each cluster detector consists of seven tapered Ge crystals, mounted in a common cryostat [16]. The total γ-ray efficiency of the set-up is about 2% at 1 MeV. Ion-γ coincidences between the ions identified with the FRS
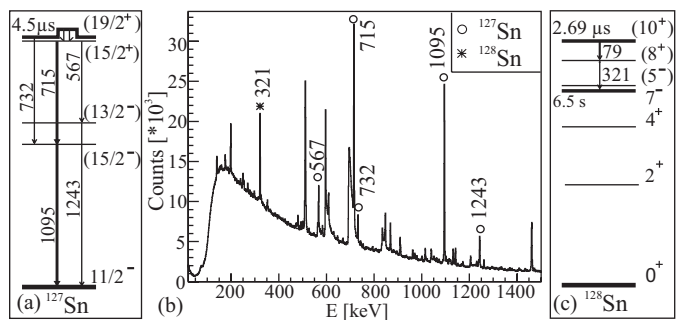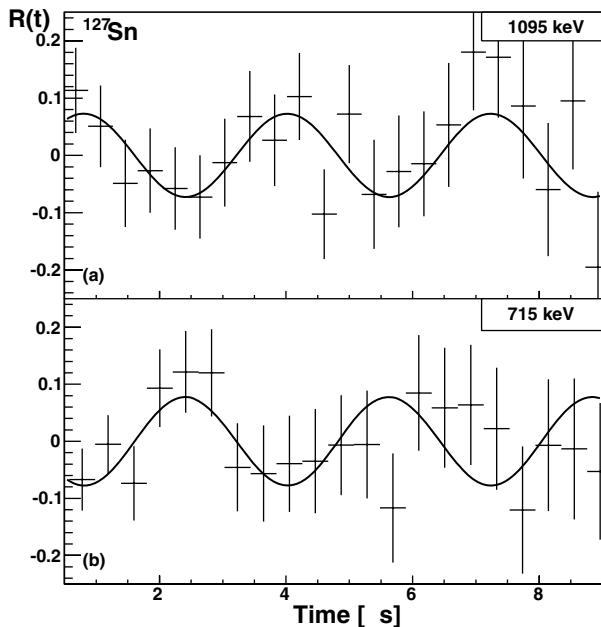
Fig. 4: $R(t)$-function of ^{127}Sn for the 1095 keV (a) and the 715 keV (b) transition at the wing of the momentum distribution.

Fig. 5: $R(t)$-function for the 321 keV transition of ^{128}Sn.

Table 1: Experimental g-factors for single-particle (s.p.) states in the Sn isotopes and empirical g-factors for the $19/2^+$ state.

s.p. config.	g_{exp}	$19/2^+$ config.	g_{emp}
$\nu(1h_{11/2}^{-1})$	$-0.242(1)$ [21]		
$\nu(3s_{1/2}^{-1})$	-2.05 [22]	$\nu(3s_{1/2}^{-1}1h_{11/2}^{-2})$	-0.156
$\nu(2d_{3/2}^{-1})$	$+0.505(3)$ [21]	$\nu(2d_{3/2}^{-1}1h_{11/2}^{-2})$	-0.266
$\nu(2d_{5/2}^{-1})$	$-0.432(2)$ [23]	$\nu(2d_{5/2}^{-1}1h_{11/2}^{-2})$	-0.241
$\nu(1g_{7/2}^{-1})$	$+0.195(3)$ [22]	$\nu(1g_{7/2}^{-1}1h_{11/2}^{-2})$	-0.230

where $A_2(\gamma)$ is the angular-distribution coefficient, depending on the spin and multipolarity of the γ-rays, B_2 is the orientation parameter, depending on the degree of alignment produced in the reaction and ϵ is a normalization coefficient. The 4th and higher-order terms were neglected, because their contribution is about one order of magnitude smaller. The amplitude of the $R(t)$-function depends on the magnitude of the spin alignment of the isomeric ensemble through the orientation parameter B_2.

To reduce systematic errors, it is customary to compose $R(t)$-functions using data from the same detector for two opposite directions of the magnetic field [20]. The following detector combinations were used (see fig. 1 for the detector labels): $I_1 = (A+L)\uparrow +(D+G)\downarrow$ and $I_2 = (A+L)\downarrow +(D+G)\uparrow$, where $\uparrow$ and $\downarrow$ denotes opposite (up and down) directions of the applied field. In addition, γ-rays detected by detectors B, C and J, K, which are placed at less sensitive angles, were used in the analysis [13]. $R(t)$-functions for isomeric decay γ-rays of ^{127,128}Sn are presented in fig. 4(a), (b) and fig. 5, respectively. After introducing the momentum selection, about 10^4 ion-γ coincidence events were used in the analysis of each of the transitions presented in figs. 4 and 5. Useful data could be obtained only for relatively long times, typically few hundred ns after the prompt event, due to the atomic bremsstrahlung caused by the stopping of the high-energy $(300\,\text{MeV}/A)$ ions in the stopper. Even though the TDPAD method is generally applicable to isomeric states with lifetimes in the $\tau = 10\,\text{ns}-10\,\mu\text{s}$ range, this "prompt flash" and the detector response effectively limit the applicability range to about $1\,\mu\text{s}$ and longer when working with relativistic ions under similar conditions.
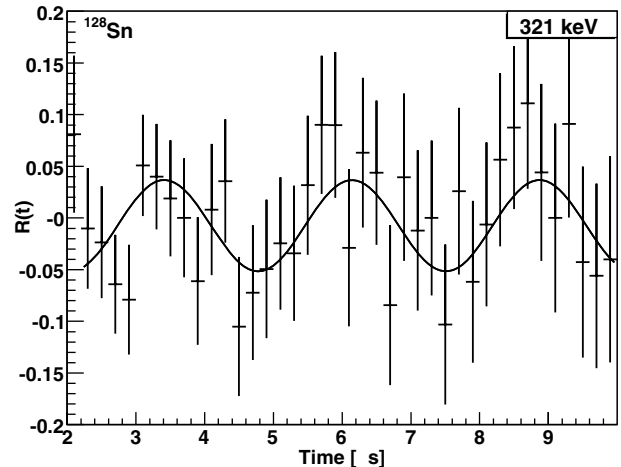
The phase of the $R(t)$-function for the 1095 keV, $(15/2^-) \to (11/2^-)$, stretched, $E2$ transition in ^{127}Sn corresponds to a negative sign of the g-factor. The sign has been deduced from the known direction of the magnetic field, assuming negative alignment in the wing of the momentum distribution, which is in line with the measured values [5] and the predictions of the kinematical fragmentation model [2,24]. The 715 keV transition in ^{127}Sn is a mixed $E1/M2$ transition suggested to connect levels with different parities, $(15/2^+) \to (15/2^-)$ and displays an opposite phase compared to the 1095 keV transition. The phase of the $R(t)$-function for the 321 keV $8^+ \to 7^-$ stretched $E1$ transition in ^{128}Sn, which is measured in the centre of the momentum distribution, also corresponds to a negative sign of the g-factor.

The fit of the $R(t)$-functions yields $g(19/2^+;\ ^{127}\text{Sn}) = -0.17(2)$ and $g(10^+;\ ^{128}\text{Sn}) = -0.20(4)$. The relatively large uncertainties are due to the fact that the number of isomeric γ-rays used in the analysis, $\sim 10^4$, is rather low. However, the present results provide a feasibility proof for such experiments. Future improvements in beam intensity and rate-hardened plastic scintillators can result in more accurate results in even farther-from-stability nuclei.

The amplitude of the $R(t)$-function

$$a = \frac{3A_2B_2}{4 + A_2B_2} \qquad (2)$$

Table 2: Experimental and calculated isomeric *g*-factors for the Sn isotopes.

	I^π	g_{exp}	SM I		SM II	
			g_{free}	g_{eff}	g_{free}	g_{eff}
^{125}Sn	$19/2^+$		-0.214	-0.150	-0.190	-0.133
^{127}Sn	$3/2^+$	$+0.505(3)$ [21]	$+0.933$	$+0.653$	$+0.737$	$+0.516$
	$11/2^-$	$-0.242(1)$ [21]	-0.371	-0.260	-0.342	-0.239
	$19/2^+$	$-0.17(2)^a$	-0.212	-0.148	-0.178	-0.125
^{129}Sn	$19/2^+$		-0.184	-0.129	-0.166	-0.116
^{124}Sn	10^+		-0.349	-0.246	-0.337	-0.236
^{126}Sn	10^+		-0.355	-0.249	-0.340	-0.238
^{128}Sn	8^+		-0.361	-0.253	-0.343	-0.240
	10^+	$-0.20(4)^a$	-0.359	-0.251	-0.344	-0.241
^{130}Sn	10^+		-0.364	-0.255	-0.348	-0.244

^{a} Present work.

was deduced as $a = 0.060(15)$ in the case of the 1095 keV transition in ^{127}Sn, which is assumed as a stretched quadrupole transition. This results in an alignment of $-19(5)\%$ in the wing of the momentum distribution, compared to a fully oblate-aligned spin ensemble. The amplitude of the $R(t)$-function of the 312 keV $8^- \to 7^-$ transition in ^{128}Sn (stretched $E1$) is $a = 0.044(16)$, which corresponds to an alignment of $+12(4)\%$ in the centre of the momentum distribution, compared to a fully prolate-aligned spin ensemble.

Discussion. –

^{127}Sn. The excitation energies of the $19/2^+$ isomers in the Sn isotopes display a similar trend to those of the 5^- states in the neighbouring even-even Sn isotopes [10]. The wave function of the 5^- isomers is suggested as an admixture of $\nu(3s_{1/2}^{-1}1h_{11/2}^{-1})$ and $\nu(2d_{3/2}^{-1}1h_{11/2}^{-1})$ terms, the former being the dominant one, as confirmed by *g*-factor measurements for ^{116,118,120}Sn, $g(5^-, \mathrm{Sn}) \approx -0.066$ [22]. Similarly, the main component of the wave function of the $19/2^+$ isomers is accepted as $\nu(3s_{1/2}^{-1}1h_{11/2}^{-1})$ with an admixture of $\nu(2d_{3/2}^{-1}1h_{11/2}^{-2})$ [11]. In addition, a $\nu(1g_{7/2}^{-1}1h_{11/2}^{-2})$ admixture was suggested in the $19/2^+$ wave function [11], for the explanation of the existence of the 15% 732 keV, $(19/2^+) \to (15/2^-)$, stretched, $M2$ transition (fig. 3(a)). Because of the L-forbiddenness, this transition cannot take place between states with the $\nu(3s_{1/2}^{-1}1h_{11/2}^{-2})$ or $\nu(2d_{3/2}^{-1}1h_{11/2}^{-2})$ and the $\nu 1h_{11/2}^{-3}$ configurations. It can have $M2/E3$ multipolarity, which in turn will involve a $\nu(2d_{5/2}^{-1}1h_{11/2}^{-2})$ admixture in the $19/2^+$ wave function.

The empirical *g*-factors for these configurations, calculated using the experimental *g*-factors for one-quasiparticle states in the Sn isotopes, are presented in table 1. The *g*-factor values for the $\nu 3s_{1/2}^{-1}$, $\nu 2d_{5/2}^{-1}$ and the $\nu 1g_{7/2}^{-1}$ states are known for lighter Sn isotopes.

The measured *g*-factor $g(19/2^+,\,^{127}Sn) = -0.17(2)$ is in good agreement with the suggested main component of

the wave function. Within the experimental uncertainty, some configuration mixing might be expected.

^{128}Sn. The 10^+ isomers in the Sn nuclei are suggested to have the $\nu 1h_{11/2}^{-2}$ configuration. The 10^+ microsecond isomer in ^{128}Sn decays to the 8^+ state with a stretched $E2$ transition, which in turn decays via a stretched $E1$ transition to the 7^- isomer ($T_{1/2} = 6.5\,\mathrm{s}$) [12].

The main configuration of the 7^- states in the even-mass Sn nuclei is $\nu(2d_{3/2}^{-1}1h_{11/2}^{-1})$. A detailed study of the *g*-factor of this isomer revealed the necessity to consider core-polarization configurations for the $M1$ operator in this region, originating from excitations across the $N = 82$ and $Z = 50$ shells [25].

The 10^+ and 8^+ states are part of $\nu 1h_{11/2}^{-2}$, seniority $\nu = 2$ multiplet. As there are two neutrons on the same orbital, the *g*-factor of such a configuration is independent of the total spin to which they are coupled and $g_{emp}(\nu 1h_{11/2}^{-2}) = g_{exp}(\nu 1h_{11/2}^{-1}; \mathrm{Sn}) = -0.24$ is expected. This value is an average of the measured *g*-factors in the neighbouring odd-*A* Sn isotopes. An average value of $g(10^+; \mathrm{Sn}) \approx -0.24$ [22] was measured for the 10^+ states in ^{116,118}Sn. The *g*-factor, $g(10^+,\,^{128}Sn) = -0.20(4)$, measured in this experiment is in agreement with these values, but within the observed experimental uncertainty some admixtures originating from core-polarizing excitations might be present in this case, too.

Shell model calculations. Shell model analysis was done starting from two different closed cores. The first model (SM I) assumes ^{132}Sn as a closed core and uses a model space for neutron holes in $3s_{1/2}, 2d_{3/2}, 2d_{5/2}$ and $1g_{7/2}$ from the $N = 4$ shell plus the intruder $1h_{11/2}$ from the $N = 5$ shell. The realistic nucleon-nucleon potential derived from modern meson exchange models was renormalized taking into account the specific nuclear medium to produce the nuclear reaction G-matrix, which was the starting point for a perturbative many-body scheme for deriving shell model interactions [26]. The calculations were done using the CENS software [27]. The experimental

single-hole energies for the orbitals are taken from ^{131}Sn. Calculations of the low-lying levels of ^{127}Sn and ^{129}Sn with the same effective interaction were presented in ref. [28] and the results are in a good agreement with the experimental data.

The second model assumes ^{88}Sr as an inert core and uses the model space for protons $2p_{1/2}, 1g_{9/2}$ and for neutrons $1g_{7/2}, 3s_{1/2}, 2d_{5/2}, 2d_{3/2}, 1h_{11/2}$ [29], *i.e.* the Sn valence space is the same as in SM I. Non-truncated shell model calculations (SM II) were recently performed for the whole Sn region down to ^{124}Sn, using a realistic two-body CD-Bonn interaction according to the method described in ref. [28]. Effective $M1$ operators as described above were used, and calculations were performed with the OXBASH code [30]. The interaction was monopole tuned to reproduce the ^{131}Sn single-hole energies. The calculations of the levels of odd Sn isotopes with the same effective interaction were presented in ref. [31].

Results with both models for g-factors of single-particle states in ^{127}Sn, $19/2^+$ isomers in the odd-A ^{125,127,129}Sn isotopes and 10^+ isomers in even-even ^{124,126,128}Sn isotopes, together with the experimental values, are shown in table 2. Values denoted as g_{free} are calculated with the g-factors for free nucleons, the g_{eff} values are calculated with the effective nucleon g-factors $g_s = 0.7 \cdot g_s^{free}$.

Based on the occupation numbers, the shell model analysis supports the suggested main component of the wave function of the $19/2^+$ isomer. In general, the calculated effective g-factors within both approaches are in agreement with the experimental values. The small differences between the calculated values are mainly due to the different cores, and perhaps to the fact that SM II uses monopole modified interactions.

The calculated g-factors for the 10^+ isomer in ^{128}Sn within both approaches are in a good agreement with the experimental value. The calculations demonstrate an amazing stability for the g-factor value of this state for the $^{124-130}$Sn isotopes. Both approaches reproduce well the g-factors of the $\nu 2d_{3/2}$ and $\nu 1h_{11/2}$ states, but somewhat underestimate the measured g-factor for the $19/2^+$ isomer in ^{127}Sn, when the effective nucleon g-factors are used. This can be due to a $\nu 2d_{5/2}$ admixture in the wave function, 4.7% and 3.5% for SM I and SM II, respectively. It allows a large non-diagonal $\nu 2d_{5/2} \rightarrow \nu 2d_{3/2}$ spin-flip matrix element, a core-polarization contribution that should already be accounted for in the adopted g_s quenching.

Summary. – The measured experimental values for the g-factors of the $19/2^+$ and the 10^+ isomers in ^{127}Sn and ^{128}Sn, respectively, confirm the shell model picture for these nuclei. The experiment provides evidence that the wave functions of these nuclei, which lie close to the doubly magic $^{132}_{50}$Sn$_{82}$, are rather pure. The success of the present technique using relativistic fragments paves the way to measurements of nuclei farther from stability in this mass region.

$$* * *$$

REFERENCES

[1] Talmi I., *Simple Models of Complex Nuclei, The Shell Model and the Interacting Boson Model* (Harwood Academic Publishers, New York) 1993.
[2] Asahi K. *et al.*, *Phys. Rev. C*, **43** (1991) 456.
[3] Schmidt-Ott W. D. *et al.*, *Z. Phys. A*, **350** (1994) 215.
[4] Georgiev G. *et al.*, *J. Phys. G*, **28** (2002) 2993.
[5] Matea I. *et al.*, *Phys. Rev. Lett.*, **93** (2004) 142503.
[6] Vermeulen N. *et al.*, *Phys. Rev. C*, **75** (2007) 051302(R).
[7] Gaudefroy L. *et al.*, *Phys. Rev. Lett.*, **102** (2009) 092501.
[8] Wollersheim H. J. *et al.*, *Nucl. Instrum. Methods A*, **537** (2005) 637.
[9] Neyens G. *et al.*, *Acta Phys. Pol. B*, **40** (2007) 1237.
[10] Pinston J. A. and Genevey J., *J. Phys. G*, **30** (2004) R57.
[11] Pinston J. A. *et al.*, *Phys. Rev. C*, **61** (2000) 024312.
[12] Fogelberg B. *et al.*, *Nucl. Phys. A*, **352** (1981) 157.
[13] Atanasova L. *et al.*, in *Proceedings of the XXV International Nuclear Theory Workshop, Rila Mountains, Bulgaria*, edited by Dimitrova S. (Diomira, Sofia) 2006, p. 161.
[14] Atanasova L. *et al.*, *Prog. Part. Nucl. Phys.*, **59** (2007) 355.
[15] Geissel H. *et al.*, *Nucl. Instrum. Methods B*, **70** (1992) 286.
[16] Eberth J. *et al.*, *Nucl. Instrum. Methods A*, **369** (1996) 135.
[17] Grebosz J., *Comput. Phys. Commun.*, **176** (2007) 251.
[18] http://root.cern.ch/drupal/.
[19] Goldring G. and Hass M., in *Treatise on Heavy Ion Science,* Vol. **3**, edited by Bromley D. Allan (Plenum, New York) 1985, p. 539.
[20] Georgiev G. *et al.*, *Eur. Phys. J. A*, **30** (2006) 351.
[21] Le Blanc F. *et al.*, *Phys. Rev. C*, **72** (2005) 034305.
[22] Stone N. J., *At. Data Nucl. Data Tables*, **90** (2005) 75.
[23] Eberz J. *et al.*, *Z. Phys. A*, **326** (1987) 121.
[24] Daugas J. M. *et al.*, *Phys. Rev. C*, **63** (2001) 064609.
[25] Ilie G. *et al.*, *Phys. Lett. B*, **687** (2010) 305.
[26] Hjorth-Jensen M. *et al.*, *Phys. Rep.*, **261** (1995) 125; Dean D. J. *et al.*, *Prog. Part. Nucl. Phys.*, **53** (2004) 419.
[27] Engeland T. *et al.*, *The CENS Software, a Computational Environment for Nuclear Structure*, http://www.fys.uio.no/compphys/cp/software.html.
[28] Gausemel H. *et al.*, *Phys. Rev. C*, **69** (2004) 054307.
[29] Grawe H., in preparation (2010).
[30] Brown B. A. *et al.*, Oxbash for Windows, MSU-NSCL report No. 1289, 2004.
[31] Lozeva R. *et al.*, *Phys. Rev. C*, **77** (2008) 064313.